Optimization of the chromone scaffold through QSAR and docking studies: Identification of potent inhibitors of ABCG2

Emile Roussel, Viet-Khoa Tran-Nguyen, Khalid Bouhedjar, Mohamed Abdesselem Dems, Amine Belaidi, Brahim Matougui, Basile Peres, Ammar Azioune, Olivier Renaudet, Pierre Falson, et al.

Optimization of the Chromone Scaffold through QSAR and Docking Studies: Identification of Potent Inhibitors of ABCG2

*Emile Roussel[1,5,6#], Viet-Khoa Tran-Nguyen[1#], Khalid Bouhedjar[2,3#], Mohamed Abdesselem Dems[2,4], Amine Belaidi[2], Brahim Matougui[2], Basile Peres[1], Ammar Azioune[2], Olivier Renaudet[5], Pierre Falson[6], and Ahcène Boumendjel[1]**

[1] Univ. Grenoble Alpes, CNRS, DPM UMR 5063, F-38041, Grenoble, France

[2] Centre de recherche en biotechnologie (CRBt), BP 73 UV 03, Ali Mendjeli Nouvelle ville – Constantine, Algeria

[3] Laboratoire de Synthèse et Biocatalyse Organique, Département de Chimie, Faculté des Sciences, Université Badji Mokhtar Annaba, BP 12, 23000 Annaba, Algeria

[4] Laboratoire de chimie des matériaux et des vivants, Univ Hadj-Lakhdar Batna, Algeria

[5] Univ. Grenoble Alpes, CNRS, DCM UMR 5250, F-38041, Grenoble, France

[6] Drug Resistance Mechanisms and Membrane Proteins Laboratory, BMSSI UMR 5086 CNRS/Université Lyon 1, Institut de Biologie et Chimie des Protéines, Lyon, France

[#] Equally contributed to this work

* Corresponding author: Pr. Ahcène Boumendjel (ahcene.boumendjel@univ-grenoble-alpes.fr)

Abstract

The membrane transporter BCRP/ABCG2 has emerged as a privileged biological target for the development of small compounds capable of abolishing multidrug resistance. In this context, the chromone skeleton was found as an excellent scaffold for the design of ABCG2 inhibitors. With the aims of optimizing and developing more potent modulators of the transporter, we herewith propose a multidisciplinary medicinal chemistry approach performed on this promising scaffold. A quantitative structure-activity relationship (QSAR) study on a series of chromone derivatives was first carried out, giving a robust model that was next applied to the design of 13 novel compounds derived from this nucleus. Two of the most active according to the model's prediction, namely compounds **22** (5-((3,5-dibromobenzyl)oxy)-*N*-(2-(5-methoxy-1*H*-indol-3-yl)ethyl)-4-oxo-4*H*-chromene-2-carboxamide) and **31** (5-((2,4-dibromobenzyl)oxy)-*N*-(2-(5-methoxy-1*H*-indol-3-yl)ethyl)-4-oxo-4*H*-chromene-2-carboxamide), were synthesized and had their biological potency evaluated by experimental assays, confirming their high inhibitory activity against ABCG2 (experimental EC_{50} below 0.10 µM). A supplementary docking study was then conducted on the newly designed derivatives, proposing possible binding modes of these novel molecules in the putative ligand-binding site of the transporter and explaining why the two aforementioned compounds exerted the best activity according to biological data. Results from this study are recommended as references for further research in hopes of discovering new potent inhibitors of ABCG2.

Keywords. Chromone, ABCG2, inhibitor, QSAR, docking, membrane transporter, predictive model.

1. Introduction

The breast cancer resistance protein (BCRP) is a membrane protein involved in drug efflux and anticancer chemotherapy failures **[1-3]**. It belongs to the subclass G of the ATP-binding cassette (ABC) protein superfamily. The overexpression of BCRP/ABCG2 at the membrane cancer cells is closely linked to the pivotal role in the transport (efflux) of a wide range of chemically unrelated chemotherapeutic agents out of the cancer cells **[4]**. Since its discovery in 1998, ABCG2 has emerged as a privileged target for the development of inhibitors used as adjuvants with clinically administered anticancer drugs with the aims of making cancer cells more sensitive to chemotherapeutics. To this end, extensive research on ABCG2 has been carried out, paving the way for a discovery of potent and selective modulators of this transporter. In this context, the chromone (4*H*-chromen-4-one, 4*H*-1-benzopyran-4-one) skeleton was early discovered as a promising scaffold for designing novel ABCG2 inhibitors (**Figure 1**). Being multifunctionable, it offers a huge opportunity for chemical modifications. Our work led us to a series of chromone derivatives with high inhibitory activities against ABCG2, also with notable selectivity towards this protein **[5,6]**. The lead compound, MBL-II-141 (**Figure 1**), has shown a promising *in vivo* activity when tested on preclinical animal models **[7-9]**. So far, our design was always based on the classical empiric structure-activity relationship (SAR) approach and has never been rationalized by any of the available molecular modeling methods.

In the present work, our aim is to conduct a quantitative structure-activity relationship (QSAR) study on a series of 19 chromone derivatives tested as inhibitors of BCRP, where the activities are correlated to the chemical descriptors; and to build a predictive model that would next be implemented in order to reach our twofold ultimate goal, which is: **(i)** to identify, synthesize and analyze the activity of the most active chromone derivative(s) predicted by the QSAR study; and **(ii)** to decipher the interactions between our inhibitor(s) and ABCG2.

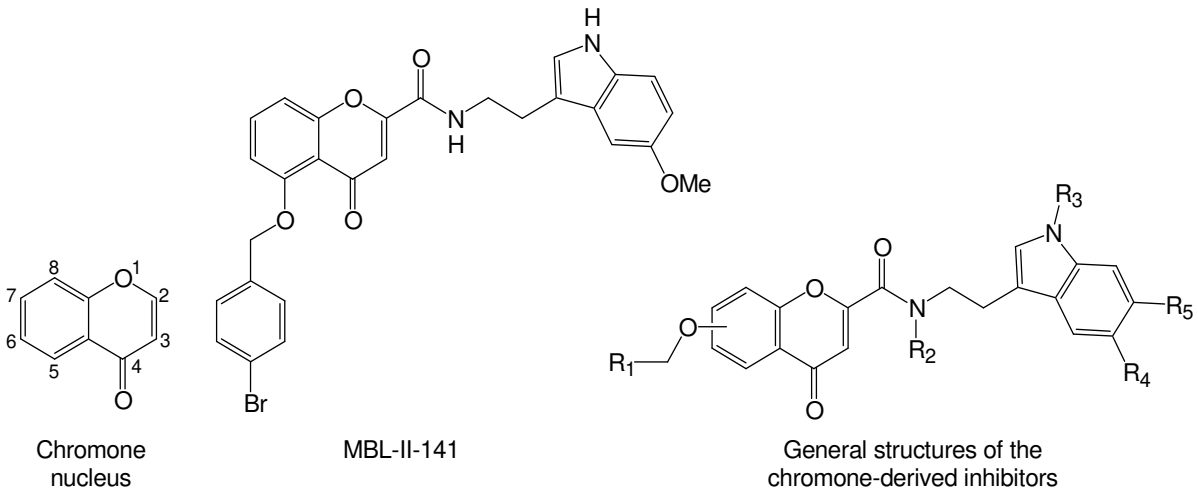

Figure 1. Structures of the chromone nucleus, the ABCG2 inhibitor MBL-II-141 and chromone-derived inhibitors investigated in this study.

2. Results and discussion

2.1. QSAR study

Chromone derivatives used in this study were previously evaluated in terms of their ability to inhibit the efflux of mitoxantrone (an anticancer drug and substrate of ABCG2) in ABCG2-transfected HEK293 cells (**Table 1**) **[5,6]**. A total of 19 selected compounds were randomly divided into a training set and a test set, with 80% of them assigned to the training set (ntr), and the remaining 20% considered as parts of the test set (nts). The inhibitory activities initially expressed as EC_{50} values (in μM) were later converted to the logarithmic scale ($pEC_{50} = -\log EC_{50}$) and were used for QSAR modeling.

The first step of this study was to develop a QSAR model that could next be used to predict the ABCG2-inhibitory activity (pEC_{50}) of a studied compound. Two theoretical molecular descriptors, *RDF140m* and *De*, were selected as the most relevant among over 3000 descriptors of different types. The first descriptor, *RDF140m*, is a radial distribution function (RDF)

descriptor (Radial Distribution Function – 14.0/weighted by atomic masses). It can be interpreted as the probability distribution of finding an atom in a spherical volume of radius R = 14.0 Å **[10]**. The second descriptor, *De*, is the D total accessibility index/weighted by atomic Sanderson electronegativity states. The stability and robustness of the models were verified by internal validations: leave-one-out (Q^2_{LOO}), leave-many-out (Q^2_{LMO}), Q^2 bootstrap. Their predictivity was also evaluated using parameters on new chemicals that were not involved in model development **[11-17]**.

Table 1. The chemical structures of 19 chromone derivatives used in the QSAR study.

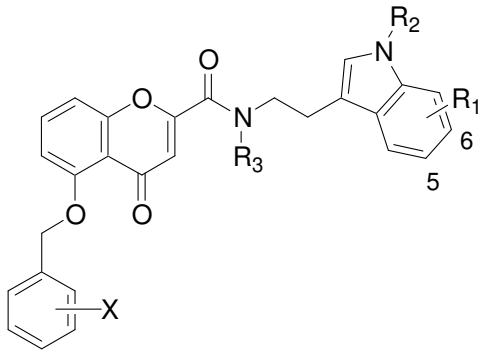

1 - 15

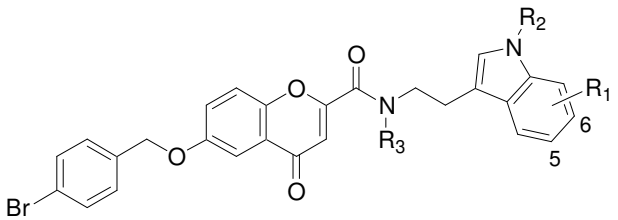

16 – 18

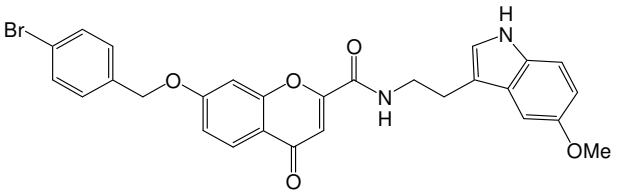

19

1	X = 4-Br, R_1 = 5-OMe, R_2 = R_3 = H	**10**	X = 4-Br, R_1 = 5-H, R_2 = R_3 = H
2	X = 2-Br, R_1 = 5-OMe, R_2 = R_3 = H	**11**	X = 4-Br, R_1 = 6-OMe, R_2 = R_3 = H
3	X = 3-Br, R_1 = 5-OMe, R_2 = R_3 = H	**12**	X = 4-Br, R_1 = H, R_2 = Me, R_3 = H
4	X = 2-F, R_1 = 5-OMe, R_2 = R_3 = H	**13**	X = 4-Br, R_1 = R_2 = H, R_3 = Me
5	X = 3-F, R_1 = 5-OMe, R_2 = R_3 = H	**14**	X = 4-Br, R_1 = H, R_2 = R_3 = Me
6	X = 4-F, R_1 = 5-OMe, R_2 = R_3 = H	**15**	X = 4-Br, R_1 = 5-OMe, R_2 = H, R_3 = Me
7	X = 3,4-difluoro, R_1 = OMe, R_2 = R_3 = H	**16**	R_1 = 5-OMe, R_2 = R_3 = H
8	X = 4-Br, R_1 = 5-OC_3H_7, R_2 = R_3 = H	**17**	R_1 = R_2 = H, R_3 = Me
9	X = 4-Br, R_1 = 5-$OCH(Me)_2$, R_2 = R_3 = H	**18**	R_1 = H, R_2 = R_3 = Me

The best performing model, namely the first *RDF140m-De* combined model (model 1), was selected by the genetic algorithm-variable subset selection (GA-VSS) approach. According to this model, the pEC_{50} value of a molecule could be predicted from the following Eq. (1). Statistical parameters related to internal and external validation (Q^2-$_{F1}$, Q^2-$_{F2}$, Q^2-$_{F3}$, CCC ext) are reported in **Table 2**.

$$pEC_{50} = 0.0872(RDF140m) - 7.081(De) + 3.464 \quad (1)$$

Table 2. Statistical parameters related to the validation of the first *RDF140m-De* combined model (model 1).

Model	Descriptors	R^2	R^2_{adj}	Q^2_{LMO}	s	F	Q^2_{LOO}	R^2_{ext}	Q^2-$_{F1}$	Q^2-$_{F2}$	Q^2-$_{F3}$	CCC ext
1	*RDF140m*, *De*	0.86	0.83	0.91	0.16	33.01	0.79	0.95	0.86	0.86	0.79	0.92

As observed in **Table 2**, the prediction ability, both internal (Q^2_{LMO}, Q^2_{LOO}) and external (Q^2-$_{F1,2,3}$, CCC ext), of the first *RDF140m-De* combined model was high, which demonstrates a satisfactory performance. **Table 3** presents a comparison between the experimental and theoretical pEC_{50} values (using Eq. (1) as formula for calculation) of all compounds used in this QSAR study, showing close results in most cases.

Table 3. The potency (experimental and theoretical) of all 19 chromone-derived compounds featured in this QSAR study in inhibiting mitoxantrone efflux by ABCG2-transfected HEK293 cells. pEC_{50} values were calculated from Eq. (1).

	Experimental pEC_{50}	Theoretical pEC_{50}
1	0.886	0.915
2	1.066	1.076
3	0.268	0.226
4	0.260	0.245
5	0.420	0.526
6	0.585	0.274
7	0.201	0.191
8	0.553	0.445
9	0.444	0.687

10	0.018	/
11	1.000	0.942
12	0.523	0.566
13	-0.045	-0.117
14	0.000	-0.112
15	0.018	-0.013
16	0.538	0.624
17	-0.412	-0.206
18	-0.314	-0.277
19	-0.104	-0.028

The Williams plot derived from the first *RDF140m-De* combined model (the right part of **Figure 2**) was used to verify the presence of outliers with cross-validated standardized residuals greater than three standard deviation units (response outliers), or with leverage values h higher than $3h^*(p + 1)/n$ (structural outliers, p is the number of variables used in the models, and $n = 15$ is the number of compounds in the training set) **[18]**. As can be observed in this plot, the compound **10** was the only response outlier. On the other hand, all compounds were located to the left of the $h^* = 0.643$ cut-off value, meaning no structural outlier was observed. In addition to the Williams plot, the graph of experimental-predicted values (the left part of **Figure 2**) is also a reference for an evaluation of this *RDF140m-De* combined model.

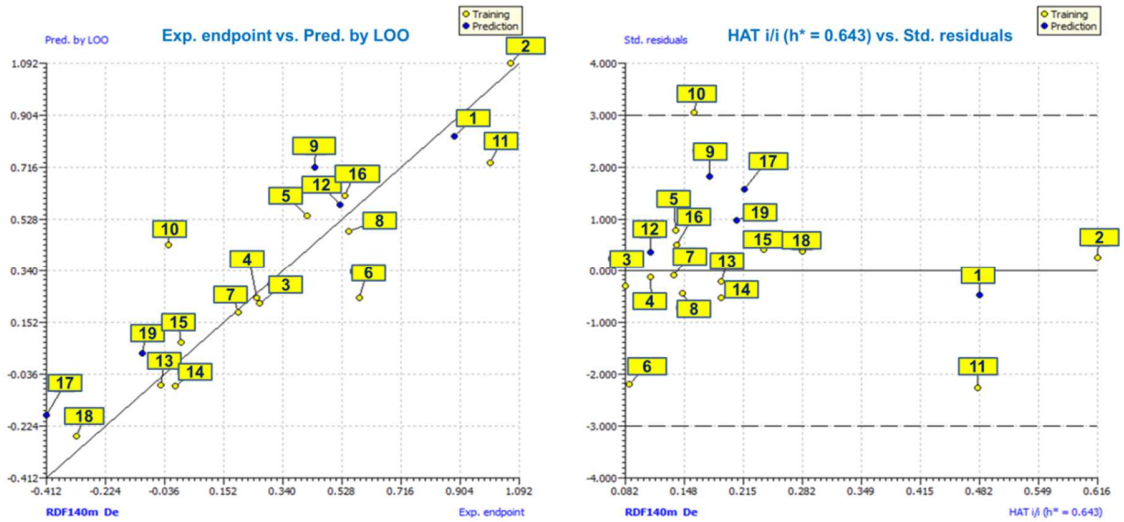

Figure 2. Graph of experimental-predicted data (left) and Williams plot (right) derived from the first *RDF140m-De* combined model.

2.2. Design of new chromone derivatives based on the predictive model

In fact, the principal aim of this paper is to develop a robust model that could be useful in conceiving new chromone derivatives with desired EC_{50} values **[19]**. To this end, the newly obtained model 2, namely the optimized *RDF140m-De* combined model, created by using two aforementioned molecular descriptors *RDF140m* and *De*, was the best combination selected by the GA-VSS approach on the ensemble of dataset previously used for the building of the first *RDF140m-De* combined model, but with the exclusion of the compound **10**, the only response outlier discussed above. Statistical parameters of this optimized model are reported in **Table 4**.

Table 4. Statistical parameters of the newly obtained optimized *RDF140m-De* combined model (model 2).

Model	Descriptors	R^2	R^2_{adj}	Q^2_{LMO}	s	F	Q^2_{LOO}	$RMSE_{tr}$	CCC cv
2	*RDF140m*, *De*	0.91	0.90	0.91	0.13	81.68	0.89	0.119	0.94

A series of 13 novel chromone-based molecules was proposed in **Table 5**. Their predicted EC_{50} values (in µM) were calculated according to the following Eq. (2), which corresponds to the newly created optimized model:

$$pEC_{50} = 0.103(RDF140m) - 5.513(De) + 2.631 \quad (2)$$

Table 5. Structures and predicted EC_{50} values (in µM) of 13 novel chromone derivatives by using the optimized *RDF140m-De* combined model and Eq. (2). The two most active compounds according to predictions (**22** and **31**) are indicated in bold.

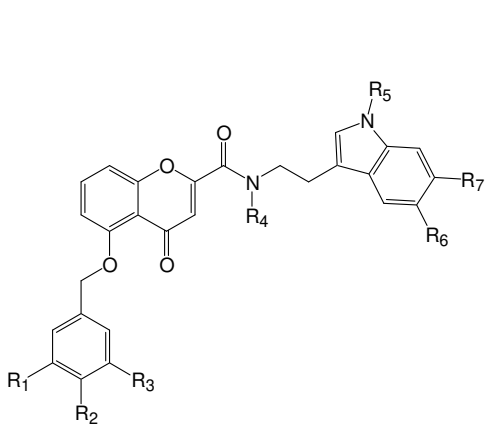

20 - 26 and 30

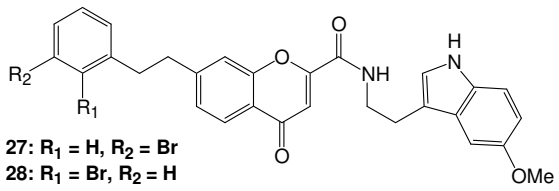

27: R_1 = H, R_2 = Br
28: R_1 = Br, R_2 = H
29: R_1 = F, R_2 = H

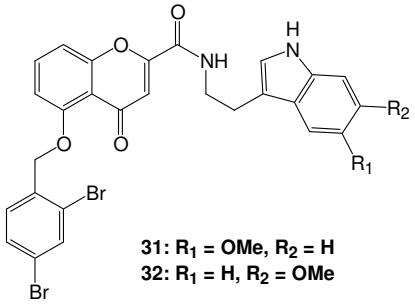

31: R_1 = OMe, R_2 = H
32: R_1 = H, R_2 = OMe

Code	R_1	R_2	R_3	R_4	R_5	R_6	R_7	Predicted EC_{50} (μM)
20	F	H	F	H	H	OMe	H	0.491
21	F	H	Br	H	H	OMe	H	0.333
22	**Br**	**H**	**Br**	**H**	**H**	**OMe**	**H**	**0.024**
23	H	F	H	H	H	H	H	0.299
24	H	Br	H	Me	Me	OMe	H	0.073
25	H	Br	H	H	H	H	OMe	0.076
26	Br	H	H	H	H	OMe	H	0.653
27								0.967
28								0.994
29								0.947
30	Br	H	Br	H	H	H	OMe	0.205
31								**0.043**
32								0.053

2.3. Chemical syntheses and BCRP-inhibitory activity testing of the best two compounds according to QSAR predictions

Compounds **22** and **31** (**Table 5**) were synthesized according to **Scheme 1**, based on our precedent method **[5,6]**. Generally, 2,6-dihydroxyacetophenone was monobenzylated by a bromo-substituted benzyl bromide. The latter was either commercially available or prepared according to known methods **[20]**. The benzylated acetophenone was subject to reaction with oxalyl chloride in the presence of sodium ethanolate (NaOEt) generated *in situ*. After an acidic treatment, the ester intermediate was isolated and directly converted into its carboxylic acid derivative. The derivative **22** was obtained using 5-methoxytryptamine (5-MT) in the presence of

benzotriazol-1-yl-oxytripyrrolidinophosphonium hexafluorophosphate (PyBOP), diisopropylethylamine (DIEA) and bis(2-oxo-3-oxazolidinyl)phosphinic chloride (BOP-Cl) during four days. The peptide coupling reaction to obtain **31** was carried out also with 5-MT but in the presence of *N,N,N′,N′*-tetramethyl-*O*-(benzotriazol-1-yl)uronium tetrafluoroborate (TBTU) and DIEA during 24 h. The desired compounds were isolated as powder that was fully characterized by means of nuclear magnetic spectroscopy (NMR) and high-resolution mass spectrometry.

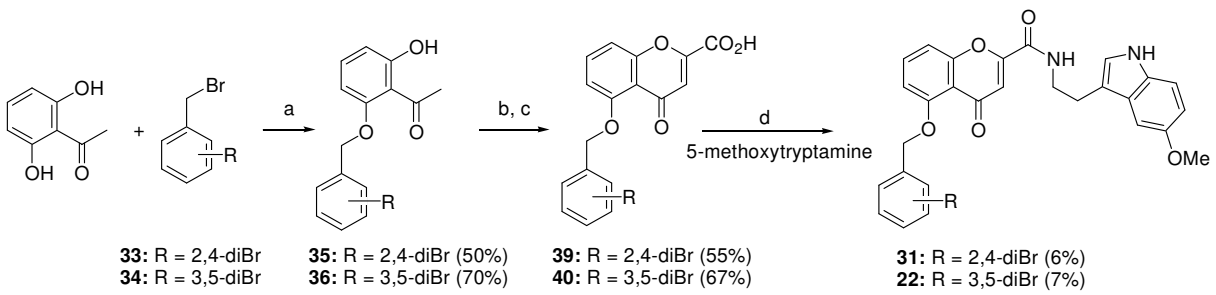

Scheme 1. (a) K_2CO_3, TBAB, acetone, reflux, 30 mins – 1 h; **(b)** NaOEt, diethyl oxalate, $EtOH_{anh}/THF_{anh}$ 1:1, 50 °C, 4 h and then, HCl (37%), reflux, 1.5 h; **(c)** K_2CO_3, THF/EtOH/H_2O 3:1:1.5, 50 °C 1.5 h; **(d) 22**: 5-methoxytryptamine, PyBOP, DIEA, DMF_{anh}, r.t., 2 days and then, BOP-Cl, r.t., 2 days; **31**: 5-methoxytryptamine, TBTU, DIEA, DMF_{anh}, r.t., 24 h.

Compounds **22** and **31** were analyzed in terms of their ability to inhibit mitoxantrone efflux and increase its accumulation in ABCG2-transfected HEK293 cells in comparison with ABCG2-negative control cells. Both compounds showed strong inhibition activities, with **31** being more active (experimental EC_{50} of **31** = 0.046 ± 0.006 μM, and of **22** = 0.097 ± 0.01 μM) (**Figure 3**). It can be observed that the experimental activity of compound **31** was in agreement with predicted data. However, the experimental EC_{50} of **22** was approximately four times higher than the value issued from the predictive model. This could be explained by the difficulty to keep the molecule solubilized during biological tests. Indeed, during the synthesis, a noticeable difference

was observed between the two compounds in terms of solubility and behaviors during the work-up and purification steps.

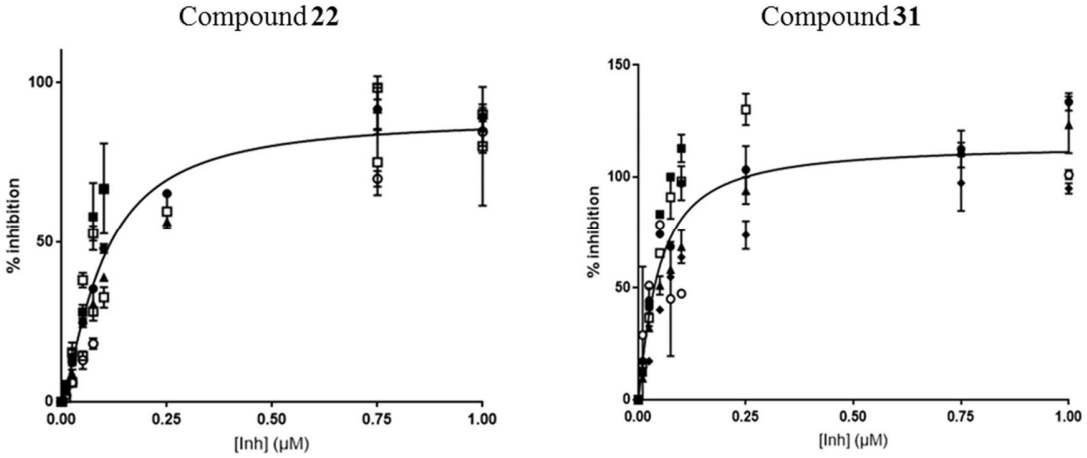

Figure 3. IC_{50} curves of compounds **22** and **31** prepared by GraphPad Prism 7.0.

2.4. Docking of investigated structures onto the putative multidrug-binding site of ABCG2

A slit-like cavity situated close to the two-fold symmetry axis of ABCG2 (PDB ID: 6FFC) was found to be a putative multidrug-binding site whose volume was almost completely, tightly and symmetrically bound by a pair of inhibitors of the transporter, preventing substrates from binding with the protein and impeding the closure of the nucleotide-binding domains, which would hamper the hydrolysis of ATP and the release of substrates to the exterior **[21]**. The cavity, accessible from both the lipid bilayer and the cytoplasmic side of the protein membrane **[21]**, is likely to optimally bind with a wide range of relatively flat, hydrophobic, polycyclic molecules **[22]**, and is composed of a series of polar and hydrophobic residues, including A397, V401, L405, T435, N436, F439, T542, with high density of hydrophobic side chains particularly found at the bottom of the cavity and in the vicinity of the membrane entrance **[21]**. The cryogenic electron microscopy (cryo-EM) pose of a molecule of MZ29 (HET code: BWQ), a

heterocyclic inhibitor of ABCG2, within the cavity is shown in **Figure 4**. The best redocked poses into the site (heavy atoms only) of the original conformation and the re-built structure (created according to our protocol described in 4.1) of this molecule obtained with PLANTS version 1.2 deviated 1.08 and 1.27 Angstroms from the true cryo-EM pose deposited on the Protein Data Bank, respectively **[23,24]**, denoting that the docking procedure managed to accurately pose the ligand and could be used for further investigation. The docking of 13 novel chromone-based molecules proposed in this study (whose structures also share some similarities with that of MZ29) was carried out into this same binding pocket. It is worth noting that the rigid docking approach was employed, with no protein side chain treated as flexible, due to the fact that the shape of ABCG2, notably of the putative multidrug-binding site, is rather compact and does not have the same flexibility in comparison to that of other transporters of the ABC superfamily **[21]**. Keeping all amino acid side chains rigid during the docking process would avoid the possible creation of unreal protein conformations that might affect (and distort) the orientation and the binding affinity of the investigated compounds inside the binding pocket.

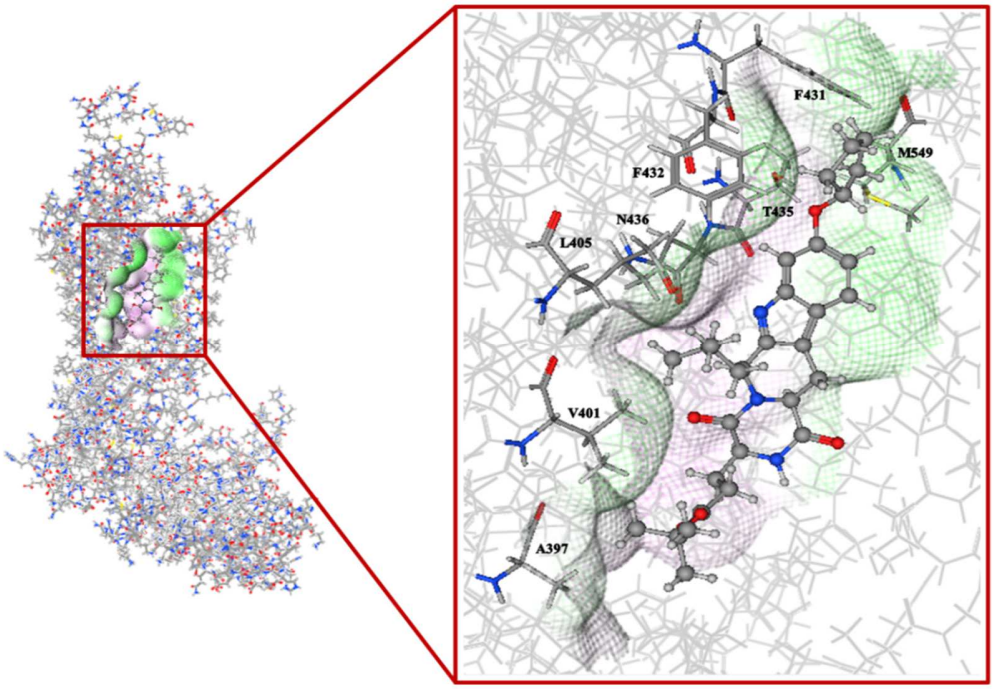

Figure 4. Cryo-EM structure of MZ29 (HET code: BWQ), an inhibitor of ABCG2 (PDB ID: 6FFC), within the putative multidrug-binding cavity of ABCG2. MZ29 is shown as balls and sticks. The molecular surface of the binding pocket is colored according to the lipophilic/hydrophilic potential of receptor atoms: purple denotes hydrophilic regions, green denotes lipophilic regions, and silver denotes neutral regions. The *O*-cyclopentyl and the *tert*-butyloxycarbonyl groups of MZ29 interact favorably with the hydrophobic residues situated at the bottom of the cavity (F431, F432, M549; shown as sticks, labeled) and in the vicinity of the membrane entrance (A397, V401, L405; shown as sticks, labeled), respectively; while the oxygen atom at the C-9 position and the NH group of the indole ring form two respective hydrogen bonds with T435 and N436 (shown as sticks, labeled).

An analysis of the best docked poses of these molecules proposes possible modes of interactions between these compounds and the putative multidrug-binding cavity of ABCG2, thus contributing to the explanation of the relevance of EC_{50} values (calculated from Eq. (2) and experimentally obtained) to the molecules' binding affinity. Each of the 13 novel chromone derivatives presented in **Table 5** generally consists of an indole moiety with a methoxy substituent at either the C-5 or the C-6 position (one exception of molecule **23**) amide-linked

with a chromone moiety with an arylmethoxy substituent at C-5, C-6 or C-7. Among these compounds, **22** and **31** (two structural isomers with a small difference in the aryl substituent on the chromone ring) gave the best predicted EC_{50} values according to Eq. (2) (calculated EC_{50} < 0.05 μM). Their potency was also confirmed by biological assays, with both experimental EC_{50} values below 0.10 μM (**31** was slightly more potent, with experimental EC_{50} < 0.05 μM).

The best docked pose of **22** and that of **31** within the putative cavity are shown in **Figure 5**. Interestingly, these two compounds were revealed to have almost identical interaction modes with the protein. Similarly to what was observed in the case of MZ29, **22**, as well as **31**, engages in two hydrogen bonds with the nearby residues T435 and N436 of the binding pocket. However, T435 now acts as a hydrogen bond donor to the arylmethoxy group's oxygen substituted on the chromone ring in each aforementioned ligand (bond length d = 2.93-3.01 Å, defined as the distance between two heavy atoms participating in the hydrogen bond, i.e. the bond donor and the bond acceptor), and N436 forms another hydrogen bond with the NH group of the amide linkage in the structures of **22** and **31** (bond length d = 2.51-2.54 Å). A stacking interaction between the phenyl ring of the residue F439 and the ligand's chromone moiety is also observed in all best docked poses of the novel compounds. Besides, the dibromophenylmethoxy substituent at the C-5 position of the chromone ring participates in van der Waals interactions with the hydrophobic residues situated at the bottom of the cavity, e.g. F431, F432. The substitution at this position allowed better interactions with both T435 and the above hydrophobic side chains, while that at C-6 (observed in compound **26**) or at C-7 (observed in **27**, **28**, **29**) resulted in an orientation of the substituent that was not favorable for a formation of a hydrogen bond with T435 and van der Waals interactions with the aforementioned residues. The binding affinities of **26**, **27**, **28** and **29** were all lower than those of **22** and **31**, and their predicted

EC_{50} values were also the highest among all novel compounds (nearly 1 μM). Moreover, the exchange of the bromine atom(s) as substituent(s) on the phenylmethoxy group with fluorine atom(s) resulted in lower binding affinities and higher calculated EC_{50} values in most cases, probably due to the mismatch with the hydrophobic side chains at the cavity bottom. Interestingly, the positions of bromine(s)/fluorine(s) on the phenyl ring (*ortho*, *meta*, *para*) seemed to have little influence on both the binding affinity and the predicted inhibition activity of studied compounds.

As observed in **Figure 5**, the indole rings of both **22** and **31** participate in van der Waals interactions with a series of residues that constitute the hydrophobic "membrane entrance" via which the cavity can be accessed from the lipid bilayer. These residues include A397, V401, and L405. A hydrogen bond is also observed between the oxygen atom in the methoxy substituent of the ligand's indole moiety and the residue S443 (bond length d = 2.91-3.05 Å), contributing to an improvement in binding affinity of the two molecules with the binding pocket. Interestingly, if the methoxy group is not substituted at the C-5 position on the indole ring, but at the C-6 position, as seen in molecule **30**, the hydrogen bond between the group's oxygen atom and S443 is no longer formed as the substituent is not oriented towards the hydroxyl group of the residue, but rather participates in much weaker hydrophobic interactions with other residues in the vicinity of the membrane entrance, which explains a lower binding affinity and an increase in the calculated EC_{50} value (from 0.024-0.043 μM to 0.205 μM). The deletion of the whole methoxy substituent, as observed in compound **23**, also resulted in a loss of interactions between the small molecule and the protein, thus leading to a decrease in predicted inhibitory potency (calculated EC_{50} = 0.299 μM). It is therefore implied that the substitution of the methoxy group at the C-5 position on the indole ring is preferable to no substitution and also to that at the C-6 position.

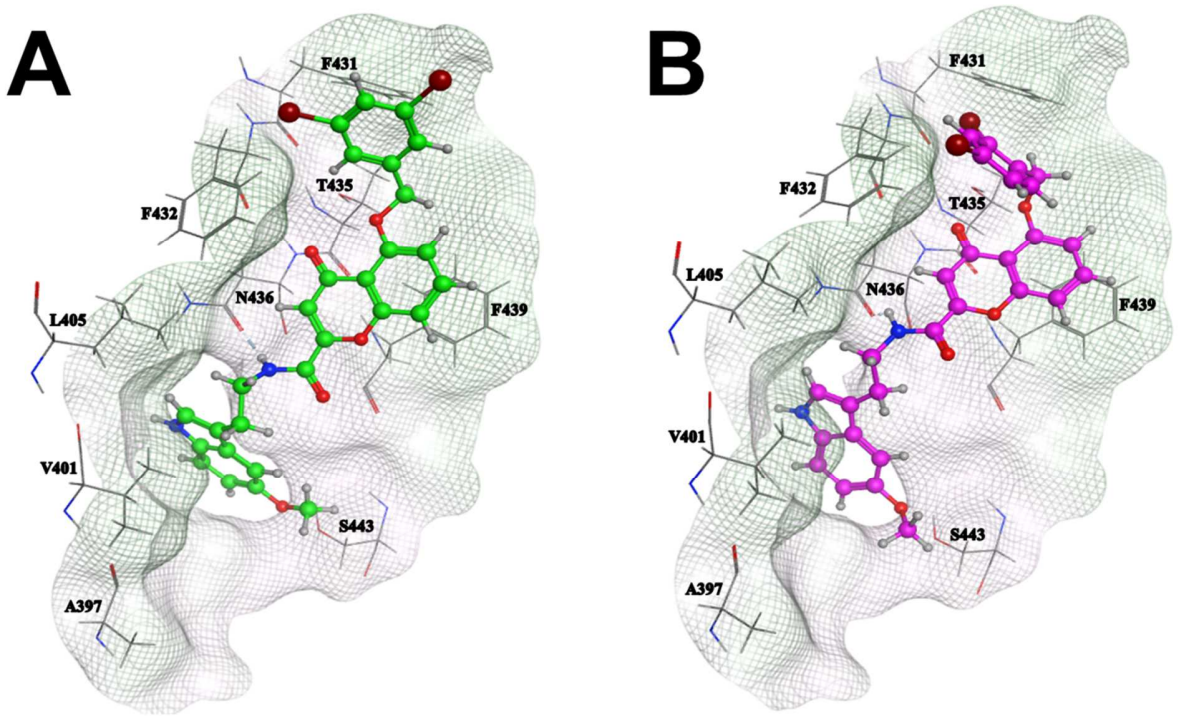

Figure 5. The best docked pose of **22 (A)** and that of **31 (B)** within the putative multidrug-binding cavity of ABCG2 showing that the 2 compounds have similar interaction modes with the protein. **22** and **31** are shown as balls and sticks. The arylmethoxy group's oxygen substituted on the chromone ring forms a hydrogen bond with T435 (shown as lines, labeled). The NH group of the amide linkage participates in a hydrogen bond with N436 (shown as lines, labeled). A stacking interaction between the phenyl ring of F439 (shown as lines, labeled) and the chromone moiety is also observed. The dibromophenylmethoxy substituent engages in van der Waals interactions with hydrophobic residues F431, F432 (shown as lines, labeled) situated at the bottom of the cavity. Other van der Waals interactions are also observed between the indole moiety and several hydrophobic side chains in the vicinity of the membrane entrance, including A397, V401, and L405 (shown as lines, labeled). Besides, the residue S443 (shown as lines, labeled) donates a hydrogen bond to the oxygen atom in the methoxy substituent of the indole ring.

The docking results of all novel compounds, in combination with their predicted EC_{50} values calculated from Eq. (2), as well as experimental data confirmed by biological assays of the two most potent compounds **22** and **31** suggest that: **(i)** the methoxy substituent should be at the C-5 position on the indole ring, **(ii)** the arylmethoxy group should be substituted at the C-5 position

of the chromone moiety, and **(iii)** the presence of bromine atom(s) as substituent(s) on the phenyl ring of phenylmethoxy is preferable to that of fluorine atom(s). These conclusions are in agreement with the EC_{50} values received from the above-mentioned QSAR dataset, with the molecule **2** featuring all the properties mentioned above and having the best pEC_{50} among all compounds in the set, both theoretically calculated using Eq. (2) (pEC_{50} = 1.076, EC_{50} = 0.084 μM) and experimentally obtained from inhibitory assays (pEC_{50} = 1.066, EC_{50} = 0.086 μM). These traits can be used as suggestions for further design of novel chromone derivatives capable of inhibiting ABCG2 in future research. Moreover, other observations made in this study, notably those regarding the binding modes of the two most potent compounds, can also pave the way for the discovery of potential inhibitors bearing other scaffolds that might mimic how our molecules interacted with certain residues of the putative ligand-binding pocket. For example, privileged scaffolds with aromatic structures, e.g. quinoline, purine, benzofuran, benzoxazole, may participate in a stacking interaction with the phenyl ring of F439 (like our compounds' chromone moiety), or engage in van der Waals interactions with hydrophobic side chains near the membrane entrance (like the indole moiety of our molecules). Multiple substituents, e.g. alkoxy/aryloxy groups with or without halogens, can be put on these scaffolds in hopes of re-creating hydrogen bonds with the key residues T435, N436, S443. Even the sulfonamide or phosphoramide structures can be employed to replace the carboxamide linkage. Once these novel molecules are designed, computational simulations would be carried out to examine their binding modes with ABCG2, their potential inhibitory activity can be predicted with the use of our proposed QSAR model, and biological assays would subsequently be conducted to confirm their potency. The promising potential of scaffold-based drug discovery that takes inspiration from the present study is therefore limitless.

3. Conclusion

Investigating the chromone scaffold has long been a promising approach towards discovering novel inhibitors of the membrane transporter BCRP/ABCG2. We herewith propose a QSAR model that was built from 19 chromone derivatives and was next applied to a set of 13 novel chromone-based molecules for a prediction of their inhibitory activity. Among them, **22** and **31** were predicted as the most potent. These compounds were later synthesized in laboratory and had their EC_{50} values confirmed by biological assays. A supplementary docking study was eventually carried out, proposing possible binding modes of the novel hits inside the ligand-binding site of ABCG2 and putting forward several suggestions in agreement with both theoretical and experimental data that could be useful for further design and development of potential modulators of the transporter. More effort would be made in our future studies to have an insight into the mechanisms of interactions between the aforementioned hits and the key residues of the binding pocket (e.g. by means of molecular dynamics simulations that take into account the internal motions of both the protein and the ligands), or to yield a crystallographic complex structure in high resolution of ABCG2 with each novel hit, and possibly, to pave the way for later discovery of new families of ABCG2 inhibitors as well as latent allosteric ligand-binding site(s) in the structure of this efflux pump. More *in vitro*, *in cellulo* and *in vivo* assays are also recommended to fully support the potential use of our two hits in anticancer therapy.

4. Experimental section

4.1. Structure preparation for QSAR and docking studies

Chromone derivative structures investigated in this study (see **Table 1** and **Table 5**, Results and Discussion) were built using the ACD/ChemSketch freeware **[25]**. A geometry optimization

step based on molecular mechanics (MM+) was carried out on all molecules, followed by parameterized model number 3 (PM3) semi-empirical quantum mechanical calculations at the final stage. All molecules were saved separately in mol2 file format.

4.2. QSAR study

More than 3000 molecular descriptors of different types (0D, 1D, 2D, 3D) representing the encoded chemical information of studied compounds were calculated using the DRAGON software **[10,26]**. For the development of QSAR models, the Ordinary Least Squares method and Genetic Algorithm-based features implemented in the QSARINS software were used to select relevant molecular descriptors among the possible candidate models **[27,28]**. The best model with the selected descriptors was obtained by the application of a GA-VSS procedure.

4.3. Chemistry

NMR spectra were recorded on a 400 MHz Bruker Avance-400 instrument (400 MHz) or on a 500 MHz Bruker Avance-500 instrument (500 MHz). Chemical shifts (δ) are reported in ppm relatively to Me_4Si used as an internal standard. Electrospray ionization (ESI) mass spectra were acquired by the Analytical Chemistry Department of Grenoble Alpes University on a Thermo Scientific ESI/LTQ Orbitrap XL instrument with a nanospray inlet. Exact mass was given in m/z. Thin-layer chromatography (TLC) was carried out using Merck silica gel F-254 plates (thickness of 0.25 mm). Unless otherwise stated, reagents were obtained from commercial sources (Alpha Aesar, Sigma-Aldrich and TCI) and were used without further purification.

4.4. Materials

DMEM (Dulbecco/Vogt modified Eagle's minimal essential medium), high glucose with GlutaMAX™ (Gibco) and fetal bovine serum (FBS, GE Healthcare Hyclone) were purchased from Fisher Scientific. Penicillin/streptomycin (10 000 U/10 mg per ml), G418, trypsine and Dulbecco's Phosphate Buffered Saline (DPBS) were purchased from Sigma Aldrich (France) as well as mitoxantrone (MX). All commercial products were of the highest available purity grade.

4.5. General procedure

All chromone derivatives were dissolved in dimethylsulfoxide (DMSO), and then diluted in DMEM high glucose medium. Stock solutions were stored at -20 °C and warmed to 25 °C just before use.

4.6. 2,4-Dibromo-1-(bromomethyl)benzene ***(33)***

2,4-Dibromotoluene (1.000 g, 4.00 mmol) and freshly purified NBS (0.925 g, 5.20 mmol) were solubilized in 12 mL of 1,2-dichloroethane under inert atmosphere. The solution was refluxed during 10 mins and azobisisobuthyronitrile AIBN, 0.328 g, 2.00 mmol) was added. The resulting suspension was stirred and refluxed during 6 h. The reaction was monitored by TLC cyclohexane 100%. Then, the reaction mixture was evaporated and a solution of cold cyclohexane/dichloromethane 1:1 was added to precipitate side products (white solid). After the filtration and evaporation, the crude product (1.476 g, 4.49 mmol) was directly used without purification.

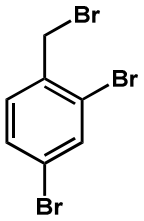

4.7. 1-(2-((2,4-Dibromobenzyl)oxy)-6-hydroxyphenyl)ethan-1-one ***(35)***

2,6-Dihydroxyacetophen-one (1.000 g, 4.00 mmol) was solubilized in 45 mL of acetone. Then, K_2CO_3 (1.659 g, 12.00 mmol) and tetra-*n*-butylammonium bromide (TBAB, 1.934 g, 6.00 mmol) were mixed together, grinded and added into the solution. The resulting suspension was refluxed during 30 mins and a solution of 2,4-dibromo-1-(bromomethyl)benzene **(33)** (1.476 g, 4.49 mmol) in 15 mL of acetone was added. The suspension was refluxed during 30 mins and then evaporated. The reaction was monitored by TLC cyclohexane/ethyl acetate 7:3. The reaction mixture was poured into ethyl acetate and acidified water (HCl 1 M) was added. The aqueous layer was extracted (3 times) with ethyl acetate and then the combined organic layers were washed (once) with acidified water (HCl 1 M) and brine. The combined organic layers were dried over $MgSO_4$, filtrated and evaporated. The crude product was precipitated thanks to a solution of cyclohexane/dichloromethane 1:1 and then crystallized in isopropanol. The desired product $C_{15}H_{12}Br_2O_3$ (0.793 g, 1.98 mmol) was obtained with 50% yield.

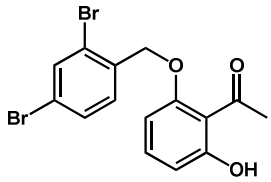

$C_{15}H_{12}Br_2O_3$. mp = 123 – 124 °C. **^{1}H NMR** (400 MHz, DMSO) δ 11.64 (s, 1H), 7.95 (d, *J* = 1.8 Hz, 1H), 7.66 (dd, *J* = 8.2, 1.8 Hz, 1H), 7.54 (d, *J* = 8.2 Hz, 1H), 7.32 (m, 1H), 6.62 (d, *J* = 8.3 Hz, 1H), 6.55 (d, *J* = 8.2 Hz, 1H), 5.13 (s, 2H), 2.45 (s, 3H). **^{13}C NMR** (101 MHz, DMSO) δ 203.27, 159.54, 157.71, 134.92, 134.60, 133.83, 132.06, 131.01, 123.92, 122.19, 114.68, 109.93, 103.16, 69.38, 32.88. **HRMS** (ESI/LTQ Orbitrap) calcd for $C_{15}H_{11}Br_2O_3$ ($M\text{-}H^+$) 396.9080, found 396.9067.

4.8. Ethyl 5-((2,4-dibromobenzyl)oxy)-4-oxo-4H-chromene-2-carboxylate ***(37)***

Sodium (0.150 g, 6.52 mmol) was solubilized in cold and dry ethanol (20 mL) to obtain a solution of sodium ethanoate. The solution was dropped into a cold solution of 1-(2-((2,4-dibromobenzyl)oxy)-6-hydroxyphenyl)ethan-1-one **(35)** (0.435 g, 1.09 mmol) in dry tetrahydrofuran (THF). Then, diethyl oxalate (0.636 g, 4.35 mmol) was added to the solution and stirred at room temperature (r.t.) during 30 mins. The resulting solution was warmed up to 50 °C and monitored by TLC cyclohexane/ethyl acetate 3:2. A precipitation of the reaction intermediate occurred during the reaction. After 4 h, drops of HCl 37% were added to the solution until the white coloration of the solid was observed. The reaction was refluxed during 1 h after color change. Then, the reaction mixture was evaporated and poured into ethyl acetate and acidified water (HCl 1 M). The aqueous layer was extracted (3 times) by ethyl acetate until discoloration. The combined organic layers were washed (once) with acidified water (HCl 1 M) and brine and then dried over $MgSO_4$ before evaporation. The oil was solidified under high vacuum and isopropanol was added and heated. The resulting suspension was filtered, and the pasty product was dissolved with dichloromethane to obtain a white solid. The desired product $C_{19}H_{14}Br_2O_5$ (0.144 g, 0.30 mmol) was obtained with 27% yield.

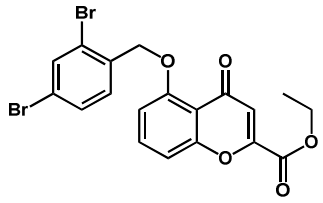

$C_{19}H_{14}Br_2O_5$. mp = 102 – 104 °C. **^{1}H NMR** (400 MHz, DMSO) δ 8.08 (d, *J* = 8.3 Hz, 1H), 7.94 (d, *J* = 1.9 Hz, 1H), 7.80 (m, 1H), 7.74 (dd, *J* = 8.3, 1.9 Hz, 1H), 7.29 (d, *J* = 8.5 Hz, 1H), 7.15 (d, *J* = 8.3 Hz, 1H), 6.81 (s, 1H), 5.19 (s, 2H), 4.40 (q, *J* = 7.1 Hz, 2H), 1.36 (t, *J* = 7.1 Hz, 3H). **^{13}C NMR** (101 MHz, DMSO) δ 176.44, 159.99, 157.23, 157.22, 150.30, 135.46, 135.43,

134.04, 130.85, 130.60, 121.82, 121.29, 115.42, 114.59, 110.90, 108.90, 69.29, 62.62, 13.87. **HRMS** (ESI/LTQ Orbitrap) calcd for $C_{19}H_{15}Br_2O_5$ ($M+H^+$) 480.9281, found 480.9271.

*4.9. 5-((2,4-Dibromobenzyl)oxy)-4-oxo-4H-chromene-2-carboxylic acid **(39)***

Ethyl 5-((2,4-dibromobenzyl)oxy)-4-oxo-4*H*-chromene-2-carboxylate **(37)** and THF (12 mL) and stirred until a complete dissolution. A solution of K_2CO_3 (0.054 g, 0.40 mmol) in 4 mL of water was added and the resulting solution was warmed up to 50 °C and stirred during 1.5 h. The reaction was monitored by TLC cyclohexane/ethyl acetate 7:3. The reaction mixture was evaporated and then solvated in dichloromethane and acidified water (HCl 1 M). In order to enhance the solubility of the desired product in the organic layer, a few drops of methanol were added. The aqueous layer was extracted (3 times) with dichloromethane and the combined organic layers were washed (once) with acidified water (HCl 1 M) and brine, then dried over $MgSO_4$, filtrated and evaporated. The solid obtained was triturated into dichloromethane and diethyl ether 1:1. The desired product $C_{17}H_{10}Br_2O_5$ (0.074 g, 0.16 mmol) was obtained with 55% yield.

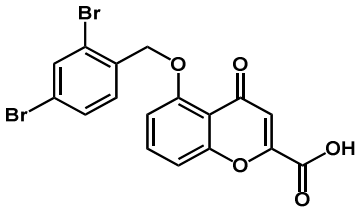

$C_{17}H_{10}Br_2O_5$. mp = 258 – 260 °C (decomposition). **^{1}H NMR** (400 MHz, DMSO) δ 8.07 (d, *J* = 8.3 Hz, 1H), 7.90 (d, *J* = 1.9 Hz, 1H), 7.76 (m, 1H), 7.70 (dd, *J* = 8.3, 1.9 Hz, 1H), 7.24 (d, *J* = 8.3 Hz, 1H), 7.10 (d, *J* = 8.3 Hz, 1H), 6.75 (s, 1H), 5.15 (s, 2H). **^{13}C NMR** (101 MHz, DMSO) δ 176.72, 161.42, 157.30, 157.17, 151.21, 135.46, 135.28, 133.97, 130.81, 130.55, 121.71, 121.23,

115.20, 114.54, 110.90, 108.69, 69.23. **HRMS** (ESI/LTQ Orbitrap) calcd for $C_{17}H_{11}Br_2O_5$ ($M+H^+$) 452.8968, found 452.8961.

4.10. 5-((2,4-Dibromobenzyl)oxy)-N-(2-(5-methoxy-1H-indol-3-yl)ethyl)-4-oxo-4H-chromene-2-carboxamide ***(31)***

5-((2,4-Dibromobenzyl)oxy)-4-oxo-4*H*-chromene-2-carboxylic acid **(39)** (0.074 g, 0.16 mmol) was solubilized in 2 mL of dry dimethylformamide (DMF). Then, DIEA (0.084 g, 0.65 mmol) and TBTU (0.105 g, 0.33 mmol) were added sequentially to the solution. After the complete dissolution, 5-methoxytryptamine (0.074 g, 0.33 mmol) was added and the resulting solution was stirred at r.t. during 24 h. The reaction was monitored by TLC cyclohexane/ethyl acetate 1:4. The reaction mixture was poured into acidified water (HCl 1 M) and extracted (3 times) with dichloromethane. The combined organic layers were washed (once) with acidified water (HCl 1 M), basified water (NaOH 10%) and brine before being dried over $MgSO_4$, filtrated and evaporated. The resulting oil was precipitated thanks to a few drops of diethyl ether. After filtration, the crude product was purified thanks to a silica column of 12 g and eluents cyclohexane/dichloromethane 4:1 followed by dichloromethane 100%. The desired product $C_{28}H_{22}Br_2N_2O_5$ (0.006 g, 0.0096 mmol), a solid, was later obtained with dichloromethane/methanol 9:1 at 6% yield.

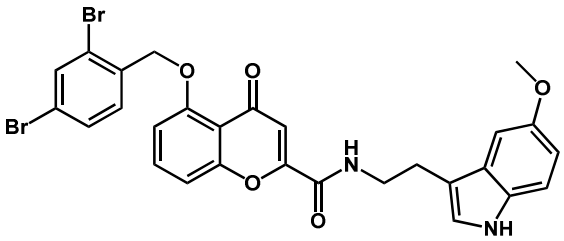

$C_{28}H_{22}Br_2N_2O_5$. mp = 276 – 277 °C (decomposition). **^{1}H NMR** (500 MHz, $CDCl_3$) δ 8.12 (d, *J* = 8.4 Hz, 1H), 8.00 (s, 1H), 7.72 (d, *J* = 1.9 Hz, 1H), 7.60 – 7.55 (m, 2H), 7.31 (d, *J* = 8.8

Hz, 1H), 7.10 (m, 2H), 7.05 (s, 1H), 6.95 – 6.89 (m, 3H), 6.85 (dd, *J* = 8.4, 0.5 Hz, 1H), 5.16 (s, 2H), 3.84 – 3.78 (m, 5H), 3.11 (t, *J* = 6.6 Hz, 2H). **^{13}C NMR** (126 MHz, $CDCl_3$) δ 177.59, 159.14, 158.11, 157.22, 154.32, 152.90, 134.78, 134.48, 134.36, 131.54, 131.28, 130.13, 127.80, 122.96, 121.80, 121.15, 115.29, 113.68, 112.63, 112.36, 112.17, 110.59, 108.41, 100.40, 69.86, 55.84, 40.52, 24.94. **HRMS** (ESI/LTQ Orbitrap) calcd for $C_{28}H_{23}Br_2N_2O_5$ ($M+H^+$) 624.9968, found 624.9950.

4.11. 1-(2-((3,5-Dibromobenzyl)oxy)-6-hydroxyphenyl)ethan-1-one ***(36)***

2,6-Dihydroxyacetophen-one (1.000 g, 4.00 mmol) was solubilized in 45 mL of acetone. Then, K_2CO_3 (1.659 g, 12.00 mmol) and TBAB (1.934 g, 6.00 mmol) were mixed together, grinded and added to the solution. The resulting suspension was refluxed during 30 mins and a solution of 1,3-dibromo-5-(bromomethyl)benzene **(34)** (1.315 g, 4.00 mmol) in 15 mL of acetone was added. The suspension was refluxed during 1 h and then evaporated. The reaction was monitored by TLC cyclohexane/ethyl acetate 7:3. The reaction mixture was solubilized with ethyl acetate and acidified water (HCl 1 M) was added. The aqueous layer was extracted with ethyl acetate (3 times) and then the combined organic layers were washed (once) with acidified water (HCl 1 M) and brine, then dried over $MgSO_4$, filtrated and evaporated. The crude product was precipitated thanks to a solution of cyclohexane/dichloromethane 1:1 and then crystallized in ethyl acetate. The desired product $C_{15}H_{12}Br_2O_3$ (1.103 g, 2.76 mmol) was obtained with 70% yield.

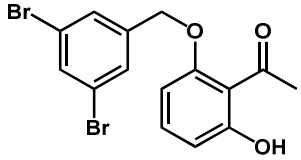

$C_{15}H_{12}Br_2O_3$. mp = 132 – 135 °C. **^{1}H NMR** (400 MHz, DMSO) δ 11.53 (s, 1H), 7.79 (s, 1H), 7.69 (d, *J* = 1.5 Hz, 2H), 7.29 (m, 1H), 6.58 (d, *J* = 8.3 Hz, 1H), 6.54 (d, *J* = 8.2 Hz, 1H), 5.17 (s, 2H), 2.53 – 2.46 (m, 5H). **^{13}C NMR** (101 MHz, DMSO) δ 203.16, 158.98, 157.30, 141.43, 133.41, 132.81, 129.45, 122.49, 115.30, 109.78, 103.40, 68.24, 32.91. **HRMS** (ESI/LTQ Orbitrap) calcd for $C_{15}H_{11}Br_2O_3$ ($M-H^+$) 396.9080, found 396.9078.

4.12. Ethyl 5-((3,5-dibromobenzyl)oxy)-4-oxo-4H-chromene-2-carboxylate ***(38)***

Sodium (0.380 g, 16.54 mmol) was solubilized in cold and dry ethanol (25 mL) to obtain a solution of sodium ethanoate. The solution was dropped into a cold solution of 1-(2-((3,5-dibromobenzyl)oxy)-6-hydroxyphenyl)ethan-1-one **(36)** (1.103 g, 2.76 mmol) in dry THF. Then, diethyl oxalate (1.612 g, 11.03 mmol) was added to the solution. The resulting solution was warmed up to 50 °C and monitored by TLC cyclohexane/ethyl acetate 7:3. A precipitation of the reaction intermediate occurred during the reaction. After 4 h, a few drops of HCl 37% were added to the solution until the white coloration of the solid was observed. The reaction was refluxed during 1.5 h after color change. Then, the reaction mixture was evaporated and poured into ethyl acetate and acidified water (HCl 1 M). The aqueous layer was extracted (3 times) by ethyl acetate until a complete discoloration. The combined organic layers were washed (once) with acidified water (HCl 1 M) and brine and then dried over $MgSO_4$ before evaporation. The solid was triturated into ethanol overnight and then filtrated. A recrystallization with ethyl acetate was possible to obtain green crystals. The desired product $C_{19}H_{14}Br_2O_5$ (0.785 g, 1.63 mmol) was obtained with 59% yield.

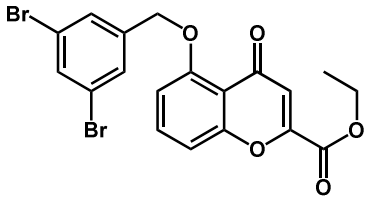

$C_{19}H_{14}Br_2O_5$. mp = 115 – 118 °C. **^{1}H NMR** (400 MHz, DMSO) δ 7.91 (d, *J* = 1.6 Hz, 2H), 7.81 – 7.74 (m, 2H), 7.26 (d, *J* = 8.1 Hz, 1H), 7.08 (d, *J* = 8.3 Hz, 1H), 6.83 (s, 1H), 5.27 (s, 2H), 4.38 (q, *J* = 7.1 Hz, 2H), 1.34 (t, *J* = 7.1 Hz, 3H). **^{13}C NMR** (101 MHz, DMSO) δ 176.55, 159.99, 157.32, 157.22, 150.28, 141.68, 135.40, 132.26, 128.38, 122.44, 115.46, 114.62, 110.82, 108.83, 68.21, 62.60, 13.86. **HRMS** (ESI/LTQ Orbitrap) calcd for $C_{19}H_{15}Br_2O_5$ ($M+H^+$) 480.9281, found 480.9274.

4.13. 5-((3,5-Dibromobenzyl)oxy)-4-oxo-4H-chromene-2-carboxylic acid ***(40)***

Ethyl 5-((3,5-dibromobenzyl)oxy)-4-oxo-4*H*-chromene-2-carboxylate **(38)** (0.785 g, 1.63 mmol) was dissolved into EtOH (17 mL) and THF (60 mL) and stirred until a complete dissolution. A solution of K_2CO_3 (0.293 g, 2.12 mmol) in 20 mL of water was added and the resulting solution was warmed up to 50 °C and stirred during 4 h. The reaction was monitored by TLC cyclohexane/ethyl acetate 7:3. The reaction mixture was evaporated and poured in acidified water (HCl 1 M) with dichloromethane. In order to enhance the solubility of the desired product in the organic layer, a few drops of methanol and THF were added. The aqueous layer was extracted (3 times), and the combined organic layers were washed (once) with acidified water (HCl 1 M) and brine, then dried over $MgSO_4$, filtrated and evaporated. The solid obtained was triturated into ethyl acetate/diethyl ether 1:2 overnight and filtrated. A recrystallization with ethyl acetate was possible to obtain white crystals. The desired product $C_{17}H_{10}Br_2O_5$ (0.493 g, 1.09 mmol) was obtained with 67% yield.

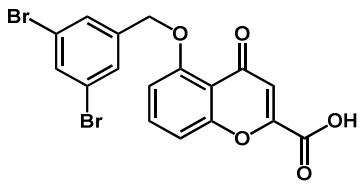

$C_{17}H_{10}Br_2O_5$. mp = 273 – 277 °C (decomposition). **^{1}H NMR** (400 MHz, DMSO) δ 7.91 (s, 2H), 7.82 – 7.72 (m, 2H), 7.24 (d, *J* = 8.4 Hz, 1H), 7.06 (d, *J* = 8.3 Hz, 1H), 6.79 (s, 1H), 5.27 (s, 2H). **^{13}C NMR** (101 MHz, DMSO) δ 176.82, 161.44, 157.31, 157.29, 151.21, 141.70, 135.23, 132.22, 128.34, 122.42, 115.23, 114.58, 110.83, 108.67, 68.19. **HRMS** (ESI/LTQ Orbitrap) calcd for $C_{17}H_{11}Br_2O_5$ ($M+H^+$) 452.8968, found 452.8958.

*4.14. 5-((3,5-Dibromobenzyl)oxy)-N-(2-(5-methoxy-1H-indol-3-yl)ethyl)-4-oxo-4H-chromene-2-carboxamide **(22)***

5-((3,5-dibromobenzyl)oxy)-4-oxo-4*H*-chromene-2-carboxylic acid **(40)** (0.100 g, 0.22 mmol) was solubilized in dry DMF (10 mL) and stirred until a complete dissolution. Then PyBOP coupling agent (0.195 g, 0.44 mmol) was added to the solution followed by DIEA (0.114 g, 0.88 mmol). The solution was stirred at r.t. during 1 h. A color change appeared. Then, 5-methoxytryptamine (0.100 g, 0.44 mmol) was added and the solution was stirred at r.t. for 2 days. Without changes in TLC cyclohexane/ethyl acetate 1:1, BOP-Cl (0.112 g, 0.44 mmol) was added to the solution. After 2 days, a TLC cyclohexane/ethyl acetate 1:1 showed the formation of products. The reaction mixture was evaporated and poured into ethyl acetate. The organic layer was washed (3 times) with basified water (K_2CO_3 saturated) then acidified water (HCl 1 M) and brine, then dried over $MgSO_4$ and evaporated to obtain a brown solid. The solid was purified by a silica column thanks to a dry sample and eluents dichloromethane 100% followed by dichloromethane/methanol 2.4:0.1. The 5 mL fractions were kept overnight under a fume

hood to precipitate the desired product after filtration. $C_{28}H_{22}Br_2N_2O_5$ (0.0068 g, 0.011 mmol) was obtained with 7% yield.

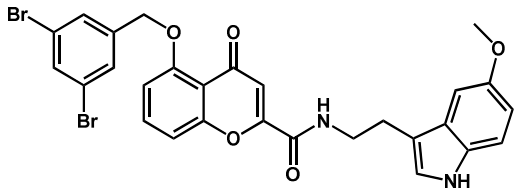

$C_{28}H_{22}Br_2N_2O_5$. mp = 285 – 288 °C (decomposition). **^{1}H NMR** (400 MHz, DMSO) δ 10.71 (s, 1H), 9.23 (t, *J* = 5.8 Hz, 1H), 7.94 (d, *J* = 1.3 Hz, 2H), 7.85 – 7.79 (m, 2H), 7.30 (d, *J* = 8.4 Hz, 1H), 7.24 (d, *J* = 8.7 Hz, 1H), 7.19 (d, *J* = 2.1 Hz, 1H), 7.12 – 7.06 (m, 2H), 6.76 – 6.70 (m, 2H), 5.30 (s, 2H), 3.75 (s, 3H), 3.58 (m, 2H), 2.97 (t, *J* = 7.4 Hz, 2H). **^{13}C NMR** (126 MHz, DMSO) δ 177.14, 159.37, 157.83, 157.49, 154.21, 153.51, 142.26, 135.54, 132.78, 131.88, 128.94, 128.03, 123.91, 122.94, 114.95, 112.57, 112.53, 111.72, 111.56, 111.36, 109.32, 100.65, 68.76, 55.81, 25.35. One signal under the solvent pic. **HRMS** (ESI/LTQ Orbitrap) calcd for $C_{28}H_{23}Br_2N_2O_5$ ($M+H^+$) 624.9968, found 624.9960.

4.15. Cell lines and cultures

ABCG2-transfected HEK293 cells, as well as their empty-plasmid counterparts, were generated as previously described **[7]**. Specifically, the ABCG2-transfected HEK293 monoclonal cell line was selected after Fluorescence-Activated Cell Sorting (FACS) using the phycoerythrin-coupled 5D3 antibody (Santa Cruz Biotech) as a native expression reporter. Cells were cultured and maintained in DMEM-High glucose with GlutaMAX™ supplemented with 10% of heat-inactivated fetal bovine serum (FBS) and 1% of penicillin/streptomycin, in a humidified atmosphere at 37 ºC with 5% CO_2. In addition, 750 µg/mL of G418 was added to the growth medium as selection agent for HEK293 transfected cells.

4.16. Inhibition tests of multidrug resistance-related drug efflux

Cells were seeded into 96-well plates at a density of 5×10^4 cells/well in 200 µL of medium and incubated overnight. Then, growth medium was switched for fresh medium containing the compounds and in the presence of 4 µM MX as a fluorescent probe for BCRP-mediated efflux to a final concentration of 0.5% DMSO (v/v). After 30 mins of incubation at 37 °C, the medium was removed, and cells were washed with 100 µL of DPBS followed by cell dissociation during 5 mins at 37 °C mediated by 25 µL of trypsin. Finally, trypsin was neutralized with 175 µL of ice-cold DPBS with 2% Bovine Serum Albumin (BSA) and the cells were carefully resuspended.

Intracellular fluorescence was measured with a MacsQUANT VRB Analyzer flow cytometer (Miltenyi Biotec) with, at least, 5.000 events recorded. MX was excited at 635 nm and fluorescence emission was recorded in a 655-730 nm window. Compounds were tested at diverse concentrations (0.010, 0.025, 0.050, 0.075, 0.10, 0.25, 0.75, 1.00 µM). The compound inhibition efficacy was estimated by using the following equation:

$$\%\ \text{inhibition} = \frac{[(G2_{FA} - G2_{FBG}) - (G2_S - G2_{FBG})]}{[(HEK_{FA} - HEK_{FBG}) - (G2_S - G2_{FBG})]} \times 100\%$$

Where $G2_{FA}$ corresponds to the fluorescence emission (a.u.) of accumulated fluorophore in cells expressing the efflux pump incubated with a fluorescent substrate and the tested compound. $G2_{FBG}$ corresponds to the resulting background fluorescence emission (a.u.) in the ABCG2-transfected cells (no substrate and no tested compound). $G2_S$ corresponds to the fluorescence emission (a.u.) of accumulated fluorophore in the cells expressing the efflux pump incubated with the substrate only. HEK_{FA} corresponds to the fluorescence emission (a.u.) of accumulated fluorophore in the control cells incubated with the substrate and the tested compound. HEK_{FBG} corresponds to the resulting background fluorescence emission (a.u.) in the control cells (no

substrate and no tested compound). All values are given as the geometric mean of fluorescence emission (a.u.) in a 655-730 nm filter (excitation 635 nm) measured in 5000 events. Assays were performed in triplicate.

4.17. Docking study

A rigid docking approach with the PLANTS software version 1.2 was carried out using the ChemPLP scoring function, the aforementioned cryo-EM structure of ABCG2 (PDB ID: 6FFC) and each of the 13 novel chromone derivatives as input (**Table 5**) **[23]**. The search speed was set at 1, enabling the highest accuracy mode. The center coordinates of the protein's ligand-binding site sphere were defined as those of the centroid of the native ligand MZ29 (HET code: BWQ) **[24]**. The sphere radius was set as the maximum distance between the binding site center and all atoms of MZ29, plus 2.0 Å. The root-mean-square deviation similarity threshold for cluster algorithm was set at 1.0 Å. Only one best pose was retained for each docking run. Other parameters were kept as default.

Acknowledgements

This work has been partially supported by CBH-EUR-GS (ANR-17-EURE-0003).

Appendix A. Supplementary data

NMR spectra of the synthesized compounds (see Experimental Section) are available in a PDF file free of charge.

Conflicts of interest

The authors declare no conflicts of interest regarding the publication of this manuscript.

Abbreviations

ABC, ATP-binding cassette; AIBN, azobisisobuthyronitrile; BCRP, breast cancer resistance protein; BOP-Cl, bis(2-oxo-3-oxazolidinyl)phosphinic chloride; Cryo-EM, cryogenic electron microscopy; DIEA, diisopropylethylamine; DMEM, Dulbecco/Vogt modified Eagle's minimal essential medium; DMF, dimethylformamide; DMSO, dimethylsulfoxide; EC_{50}, half maximal effective concentration; EtOH, ethanol; GA-VSS, genetic algorithm-variable subset selection; HRMS, high resolution mass spectroscopy; LTQ, linear trap quadrupole; MX, Mitoxantrone; NBS, *N*-bromosuccinimide; NMR, nuclear magnetic spectroscopy; PyBOP, benzotriazol-1-yl-oxytripyrrolidinophosphonium hexafluorophosphate; QSAR, quantitative structure-activity relationship; r.t., room temperature; SAR, structure-activity relationship; TBAB, tetra-*n*-butylammonium bromide; TBTU, *N,N,N′,N′*-tetramethyl-*O*-(benzotriazol-1-yl)uronium tetrafluoroborate; THF, tetrahydrofuran; TLC, thin-layer chromatography.

References

[1] R. Allikmets, L.M. Schriml, A. Hutchinson, V. Romano-Spica, M. Dean, A Human Placenta-Specific ATP-Binding Cassette Gene (ABCP) on Chromosome 4q22 That Is Involved in Multidrug Resistance, Cancer Res. 58 (1998) 5337–5339. http://cancerres.aacrjournals.org/content/58/23/5337.

[2] L.A. Doyle, W. Yang, L.V. Abruzzo, T. Krogmann, Y. Gao, A.K. Rishi, D.D. Ross, A Multidrug Resistance Transporter from Human MCF-7 Breast Cancer Cells, Proc. Natl. Acad. Sci. U.S.A. 95 (1998) 15665–15670. https://doi.org/10.1073/pnas.95.26.15665.

[3] K. Miyake, L. Mickley, T. Litman, Z. Zhan, R. Robey, B. Cristensen, M. Brangi, L. Greenberger, M. Dean, T. Fojo, Molecular Cloning of CDNAs Which Are Highly Overexpressed

in Mitoxantrone-Resistant Cells, Cancer Res. 59 (1999) 8–13. http://cancerres.aacrjournals.org/content/59/1/8.long.

[4] D. Hira, T. Terada, BCRP/ABCG2 and High-Alert Medications: Biochemical, Pharmacokinetic, Pharmacogenetic, and Clinical Implications, Biochem. Pharmacol. 147 (2018) 201–210. https://doi.org/10.1016/j.bcp.2017.10.004.

[5] G. Valdameri, E. Genoux-Bastide, B. Peres, C. Gauthier, J. Guitton, R. Terreux, S.M.B. Winnischofer, M.E.M. Rocha, A. Boumendjel, A. Di Pietro, Substituted Chromones as Highly Potent Nontoxic Inhibitors, Specific for the Breast Cancer Resistance Protein, J. Med. Chem. 55 (2012) 966–970. https://doi.org/10.1021/jm201404w.

[6] E. Winter, F. Lecerf-Schmidt, G. Gozzi, B. Peres, M. Lightbody, C. Gauthier, C. Ozvegy-Laczka, G. Szakacs, B. Sarkadi, T.B. Creczynski-Pasa, A. Boumendjel, A. Di Pietro, Structure–Activity Relationships of Chromone Derivatives toward the Mechanism of Interaction with and Inhibition of Breast Cancer Resistance Protein ABCG2, J. Med. Chem. 56 (2013) 9849–9860. https://doi.org/10.1021/jm401649j.

[7] M. Honorat, J. Guitton, C. Gauthier, C. Bouard, F. Lecerf-Schmidt, B. Peres, R. Terreux, H. Gervot, C. Rioufol, A. Boumendjel, A. Puisieux, A. Di Pietro, L. Payen, MBL-II-141, a Chromone Derivative, Enhances Irinotecan (CPT-11) Anticancer Efficiency in ABCG2-Positive Xenografts, Oncotarget 5 (2014) 11957–11970. https://doi.org/10.18632/oncotarget.2566.

[8] J. Reis, A. Gaspar, N. Milhazes, F. Borges, Chromone as a Privileged Scaffold in Drug Discovery: Recent Advances: Miniperspective, J. Med. Chem. 60 (2017) 7941–7957. https://doi.org/10.1021/acs.jmedchem.6b01720.

[9] A. Gaspar, M.J. Matos, J. Garrido, E. Uriarte, F. Borges, Chromone: A Valid Scaffold in Medicinal Chemistry, Chem. Rev. 114 (2014) 4960–4992. https://doi.org/10.1021/cr400265z.

[10] R. Todeschini, V. Consonni, Handbook of Molecular Descriptors. Methods and Principles in Medicinal Chemistry, Wiley-VCH Verlag GmbH, Weinheim, Germany, 2000. https://doi.org/10.1002/9783527613106.

[11] L.I. Lin, A Concordance Correlation Coefficient to Evaluate Reproducibility, Biometrics 45 (1989) 255–268. https://doi.org/10.2307/2532051.

[12] V. Consonni, D. Ballabio, R. Todeschini, Evaluation of Model Predictive Ability by External Validation Techniques, J. Chemom. 24 (2010) 194–201. https://doi.org/10.1002/cem.1290.

[13] N. Chirico, P. Gramatica, Real External Predictivity of QSAR Models. Part 2. New Intercomparable Thresholds for Different Validation Criteria and the Need for Scatter Plot Inspection, J. Chem. Inf. Model. 52 (2012) 2044–2058. https://doi.org/10.1021/ci300084j.

[14] N. Chirico, P. Gramatica, Real External Predictivity of QSAR Models: How to Evaluate It? Comparison of Different Validation Criteria and Proposal of Using the Concordance Correlation Coefficient, J. Chem. Inf. Model. 51 (2011) 2320–2335. https://doi.org/10.1021/ci200211n.

[15] V. Consonni, D. Ballabio, R. Todeschini, Comments on the Definition of the Q2Parameter for QSAR Validation, J. Chem. Inf. Model. 49 (2009) 1669–1678. https://doi.org/10.1021/ci900115y.

[16] G. Schüürmann, R.U. Ebert, J. Chen, B. Wang, R. Kühne, External Validation and Prediction Employing the Predictive Squared Correlation Coefficient - Test Set Activity Mean vs Training Set Activity Mean, J. Chem. Inf. Model. 48 (2008) 2140–2145. https://doi.org/10.1021/ci800253u.

[17] P. Gramatica, A. Sangion, A Historical Excursus on the Statistical Validation Parameters for QSAR Models: A Clarification Concerning Metrics and Terminology, J. Chem. Inf. Model. 56 (2016) 1127–1131. https://doi.org/10.1021/acs.jcim.6b00088.

[18] P. Gramatica, S. Cassani, P.P. Roy, S. Kovarich, C.W. Yap, E. Papa, QSAR Modeling Is Not "Push a Button and Find a Correlation": A Case Study of Toxicity of (Benzo-)Triazoles on Algae, Mol. Inform. 31 (2012) 817–835. https://doi.org/10.1002/minf.201200075.

[19] K. Roy, On Some Aspects of Validation of Predictive Quantitative Structure-Activity Relationship Models, Expert Opin. Drug Discov. 2 (2007) 1567–1577. https://doi.org/10.1517/17460441.2.12.1567.

[20] M.E. Zhidkov, O.V. Baranova, N.N. Balaneva, S.N. Fedorov, O.S. Radchenko, S.V. Dubovitskii, The First Syntheses of 3-Bromofascaplysin, 10-Bromofascaplysin and 3,10-Dibromofascaplysin - Marine Alkaloids from Fascaplysinopsis Reticulata and Didemnum Sp. by Application of a Simple and Effective Approach to the Pyrido[1,2-a:3,4-B′]Diindole System, Tetrahedron Lett. 48 (2007) 7998–8000. https://doi.org/10.1016/j.tetlet.2007.09.057.

[21] S.M. Jackson, I. Manolaridis, J. Kowal, M. Zechner, N.M.I. Taylor, M. Bause, S. Bauer, R. Bartholomaeus, G. Bernhardt, B. Koenig, A. Buschauer, H. Stahlberg, K.H. Altmann, K.P.

Locher, Structural Basis of Small-Molecule Inhibition of Human Multidrug Transporter ABCG2, Nat. Struct. Mol. Biol. 25 (2018) 333–340. https://doi.org/10.2210/pdb6ffc/pdb.

[22] N.M.I. Taylor, I. Manolaridis, S.M. Jackson, J. Kowal, H. Stahlberg, K.P. Locher, Structure of the Human Multidrug Transporter ABCG2, Nature 546 (2017) 504–509. https://doi.org/10.1038/nature22345.

[23] O. Korb, T. Stützle, T.E. Exner, Empirical Scoring Functions for Advanced Protein−Ligand Docking with PLANTS, J. Chem. Inf. Model. 49 (2009) 84–96. https://doi.org/10.1021/ci800298z.

[24] H.M. Berman, J. Westbrook, Z. Feng, G. Gilliland, T.N. Bhat, H. Weissig, I.N. Shindyalov, P.E. Bourne, The Protein Data Bank, Nucleic Acids Res. 28 (2000) 235-242. https://doi.org/10.1093/nar/28.1.235.

[25] ACD/Chem Sketch Freeware. 2015.

[26] Talete. Dragon (Software for Molecular Descriptor Calculation), Version 6.0, Milan, Italy. Talete SRL: Milan 2008.

[27] P. Gramatica, N. Chirico, E. Papa, S. Cassani, S. Kovarich, QSARINS: A New Software for the Development, Analysis, and Validation of QSAR MLR Models, J. Comput. Chem. 34 (2013) 2121–2132. https://doi.org/10.1002/jcc.23361.

[28] P. Gramatica, S. Cassani, N. Chirico, QSARINS-Chem: Insubria Datasets and New QSAR/QSPR Models for Environmental Pollutants in QSARINS, J. Comput. Chem. 35 (2014) 1036–1044. https://doi.org/10.1002/jcc.23576.

GRAPHICAL ABSTRACT

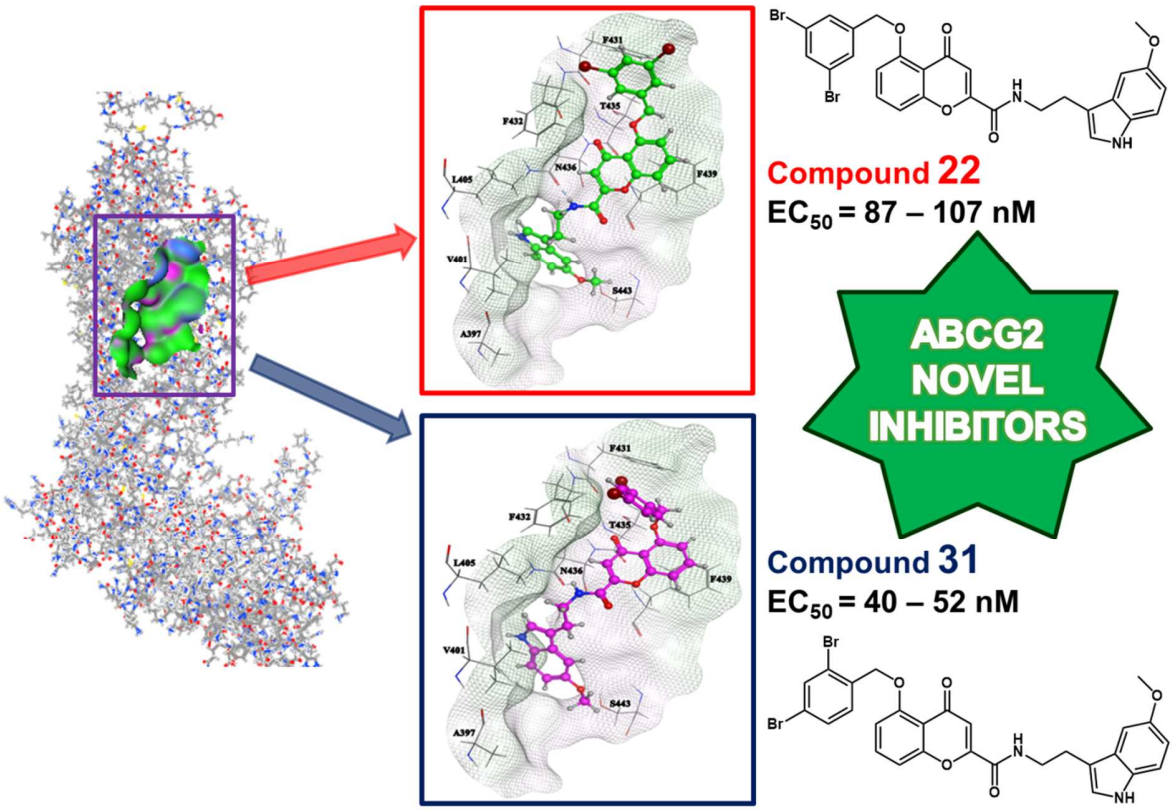

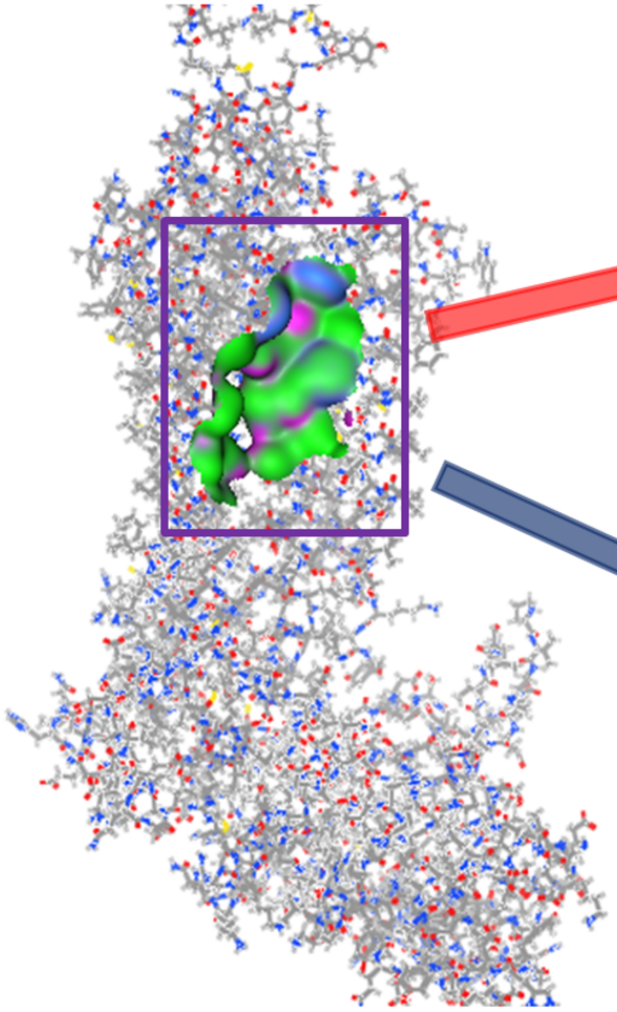

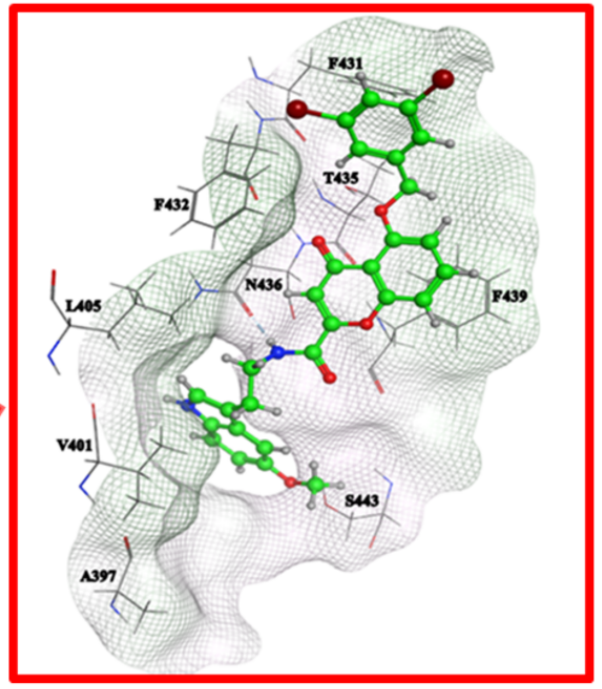

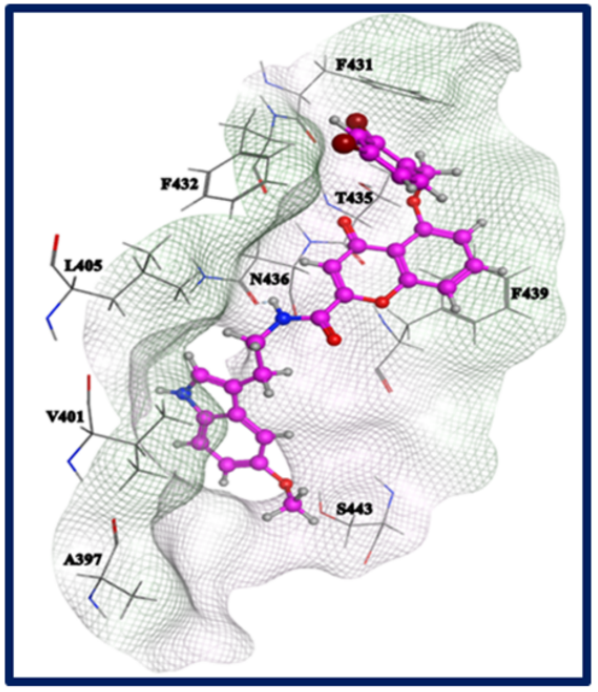

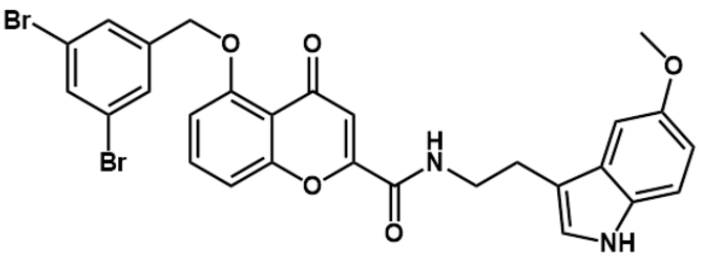

Compound 22

EC_{50} = 87 – 107 nM

ABCG2 NOVEL INHIBITORS

Compound 31

EC_{50} = 40 – 52 nM